Monitoring Deep-Sea Soundscape off the TROPIC Seamount Using a Glider

1st Hugues Chognot
LARSys, University of Algarve
Faro, Portugal
hmchognot@ualg.pt

2nd Luciano de Oliveira Junior
LARSys, University of Algarve
Faro, Portugal
lojunior@ualg.pt

3rd Rémi Emmetière
ALSEAMAR
Rousset, France
remmetiere@alseamar-alcen.com

4th Sérgio M. Jesus
LARSys, University of Algarve
Faro, Portugal
smmjesus@protonmail.com

***Abstract*—The deep-sea hosts unique ecosystems that could be threatened by emerging human activities. Within the European TRIDENT initiative, which aims to monitor environmental impacts of deep-sea exploration and exploitation, this study investigates the underwater soundscape of the TROPIC Seamount (TS), a biodiversity hotspot and a site rich in minerals.**

During a 2024 scientific cruise, an ALSEAMAR SeaExplorer glider equipped with a hydrophone that collected acoustic data along a route around TS. A method was developed to estimate ambient sound, accounting for glider self-noise and flow noise. Power spectral density (PSD) and spectral probability density (SPD) were calculated, and model validation was performed using mean square error, Kullback-Leibler, and Jensen-Shannon divergence.

Results show high-quality PSD series after self-noise removal and a clear correlation with wind speed. Flow-noise distributions are consistent with previous findings, helping analysis of recorded field at low frequencies. This work supports TRIDENT's goals and highlights the use of gliders for deep-sea acoustic monitoring.

I. Introduction

The deep-sea is one of the most untouched environment on Earth and a unique ecosystem with a biodiversity found nowhere else. In recent years, the idea to introduce exploration and exploitation activities in the deep-sea has emerged, following the interest in rare materials, and could have undesirable consequences for the environment [1] [2] [3]. The European initiative TRIDENT aims at monitoring environmental impacts of deep-sea activities [4]. Since the ambient sound is a crucial field of the ecosystem used by a large part of the fauna and now recognized as an Essential Ocean Variable, underwater sound was chosen as a key monitoring parameter. For this project, an ambient sound field baseline of the TROPIC Seamount (TS) should be defined with experimental data and a soundscape model. This seamount is located between the Canary Archipelago and Cabo Verde, the top of the TS has an approximate depth of 1000 m, and surrounding water with a depth of 4500 m. It is both a biodiversity hotspot and a site of interest for mineral exploration due to its rare mineral-rich flanks [5]. A sea campaign took place at the TS from the 13^{th} of June to the 3^{rd} of July 2024 on board the R/V Mario Ruivo, a research vessel of the Portuguese institute IPMA. During this cruise, from 20 to 27 June 2024, an ALSEAMAR SeaExplorer underwater glider was deployed with an hydrophone that recorded the ambient sound.The glider's route was planned to achieve a quarter of a circle with a 40 km radius around the TS, following the requirement of previous modelling study [6]. Here we present a method to study the ambient sound field of the TS using an underwater glider in line with previous scientific works [7] [8] [9].The proposed method takes into account the two mechanisms of glider noise generation that are self-noise and flow noise and the estimation of the power spectrum density (PSD), and the spectral probability density (SPD) of recorded tracks [10] [11] [12] [13]. A comparison of three methods of validating the soundscape model is also presented, using modelled and experimental histograms representing the probability of tracks levels hin 1/3 octave frequency bands. The 3 comparison metrics are: mean-square error, Kullback-Leibler (KL) and Jensen-Shannon(JS) divergence [14] [15]. The results obtained showed a good agreement between literature, model and data for various soundscape components.

II. Glider mission at the TS

A. Glider mission

The glider was deployed on June 21, 10 km west of the TS, which is located at the coordinate point 24°52' N, 21°42' W. Over the course of the mission, the glider performed 59 yos, e.g. couples of descent and ascent, down to a depth of 1000 m. The glider route was composed of different phases shown as red dots is Fig. 1. Phase 1: Navigate westward until reaching a location 40 km from the TS. Phase 2: Follow a quarter-circle trajectory northward. Phase 3: Moving northward until reaching a point 75 km from the TS. Phase 4: Conduct data collection over a 20 km route at a 75 km distance from the TS. Phase 5: Return to the TS for recovery. Yos that start and end a phase are circled in black with their associated number. The time of the glider's phases are shown in Table I

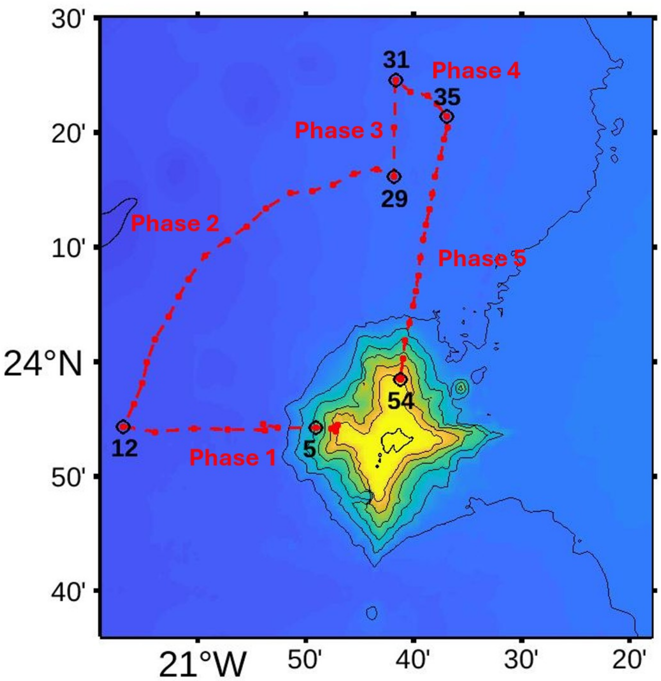

Fig. 1: SeaExplorer glider route (red). Dots represent positions between dives (called yos). Yos that start and end a phase are referred to by their associated numbers. Dashed lines between dots are approximate paths.

Phase	start date (yo)	end date (yo)
1	20/06 11:20 (5)	21/06 17:36 (11)
2	21/06 17:36 (12)	24/06 05:45 (28)
3	24/06 05:45 (29)	24/06 14:15 (30)
4	24/06 14:15 (31)	25/06 04:58 (34)
5	25/06 04:58 (35)	27/06 05:03 (54)

TABLE I: Glider mission phase date time

B. Acoustic Data

The hydrophone embedded on the glider was a single, calibrated, omni-directional hydrophone, model GTI M36-100 from GeoSpectrum Technologies Inc., placed at the glider nose section. The pre-amplifier and recorder was a PORPOISE type from Turbulent Research with a sampling frequency of $f_s = 192\,\mathrm{kHz}$. Data was recorded continuously from the start to the end of a yo in WAV data filesof a 1GB maximum size each that correspond to 31min, and saved on a $512\,\mathrm{GB}$ flashcard. The large size of acoustic files was not suitable for in situ data transfer. After the mission, to fit with the soundscape model bandwidth of 4000Hz, all the files were downsampled to $12\,\mathrm{kHz}$ which corresponds to a down sampling factor of $m = 16$. To downsample acoustic signals, we applied a 8^{th}-order low-pass Butterworth filter with cut-off frequency $\nu = fs/2M = 6000\,\mathrm{kHz}$. Additionally, a CSV noise file recorded the glider's mechanical actions during the full mission to later detect when self-generated glider noise could contaminate the acoustic signal.

C. Soundscape Model

The developed soundscape model covers a $400\,\mathrm{km}$ by $400\,\mathrm{km}$ area, centered on the TS and aims to model the sound level of the area's associated 3D grid with a surface resolution of $1\,\mathrm{km}$ and a resolution depth of $30\,\mathrm{m}$ from 30 to $970\,\mathrm{m}$. It takes as input the ocean water column CTD and the wind speed from the Copernicus database [16], the bathymetry from GEBCO [17], and marine traffic with AIS data recorded from the ship during the cruise. Ship generated noise is propagated over the area using the ray tracing model BELLHOP [18], and the JOMOPANS-ECHO ship source model; this model is based on ship characteristics, as well as empirical component based on the ECHO data set [19]. The wind noise is calculated using the Hildebrand model, that estimates the associated acoustic level at a given depth knowing the water column characteristic parameters as well as the surface wind speed [20]. The output is the acoustic power at each modelling point for 24 1/3 octave frequency bands from 1 to $4\,\mathrm{kHz}$ estimated as follow:

$$L_m(t,\mathbf{r},f) = 10\log_{10}(10^{L_w(t,\mathbf{r},f)} + \sum_{q=1}^{Q} 10^{L_{S_q}(f)/10} 10^{H(\mathbf{r}_q;t,f)/10}) \quad (1)$$

where, for each spatial location $\mathbf{r}$, time t and frequency f , the variables L_m, L_w and L_{Sq} are the sound pressure levels for the model output, the wind model and the qth ships source, respectively, and where $H(\mathbf{r}_q;t,f)$ is the transmission loss between locations $\mathbf{r}$ and $\mathbf{r_q}$, also at time t and frequency f . The locations r_q designate coordinates for ship q.

III. Methods

A. Glider-generated noise

Along the way, the glider's hydrophone records two types of sound: the one coming from the environment, called ambient sound, as well as the glider's radiated noise, which is the sound produced by the glider itself along its way. This noise is generated by two mechanisms: glider self-generated noise and flow noise. The glider self-generated noise encompasses the sound produced by its machinery, such as the ballast, battery motion, and any electrical noise coming from the glider. Those noises are transient and broadband in frequency. Self-noise is eliminated by removing periods of time specified in the noise file. Flow noise is generated by the pressure fluctuation on the hydrophone given to a turbulent fluid flow that occurs in front or behind the hydrophone [10]. This mechanism generates pseudo-noise that occurs in a low-frequency band, theoretically ranging from 0 to $500\,\mathrm{Hz}$. The sketch in Fig. 2 shows the various frequency bands with flow noise influence. The upper limit of the band variates with the water flow speed, and three frequency regions can be seen. From 0 to 20 Hz, the flow noise is dominant with a spectral probability density (SPD) following a decrease in a slope of $f^{-5/3}$. From 20 to 500 Hz flow noise and ambient noise are present, and the SPD is following a slope of f^{-m}, with m a factor that depends on the water flow the glider is facing. Higher than 500 Hz, ambient sound is dominant [12] [13]. Using a SPD draft, Fig. 2 illustrates the three regions and the way in which flow noise is distributed over the frequencies. Since soundscape model results are given for June 22, see section II-A, an estimation of the flow noise is done during glider's step 1. It consists in determining, with the estimated SPD of the selected period, the two frequencies that separate the three flow noise regions as well as the slope f^{-m}. Because the flow noise occurs at any location, all the depth layers and all the yos are used for the estimation.

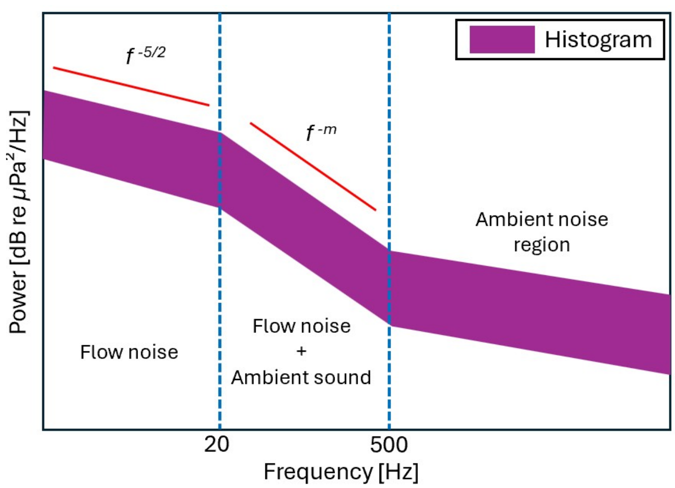

Fig. 2: Flow-noise contribution to the SPD

B. sample-PSD, PSD, SPD

After removing the self-generated noise, each track was converted into sample-PSDs following the Welch's method and using an audio segment of 12000 data samples normalized by a Hann window and a 50% overlap.

$$P_s(f) = 2\frac{[X(f)]^2}{U \cdot f_s}, \tag{2}$$

where P_s represents the sample-PSD, f the frequency, X the Fourier transform of the data segment, U the normalisation factor related to the Hann window and f_s the signal sample frequency. This sample-PSD is the basic acoustic data element to evaluate the ambient sound field, the self-noise generated by the glider, as well as the flow-noise recorded by the glider.

To examine the time dependence of the ambient sound field and validate the glider self-noise elimination. The PSD is processed by averaging sample-PSDs over a time window of 1 hour using the Welch's method. Since the overlap between two sample-PSDs is $50\,\%$ during $1\,h$ there is 6200 samples. Those contaminated by self-noise, approximately $10\,$s per hour, are removed from the PSD's estimation. As a result, each PSD is computed using approximately 5000 sample-PSDs.

To examine how the levels of a period of time (T) are distributed within a frequency band, the SPD is computed using 1-second sample-PSD. The 1^{st} the 99^{th} and each 10^{th} percentiles are calculated to represent the distribution of level occurrences across frequencies, using approximately 5000 sample-PSDs.

C. Model Validation

To compare the model against experimental data, for each phase, the SPDs are computed and converted into 1/3 octave (base 10) in 24 intervals from 15 to $4500\,$Hz by summing the power of each frequency band.

$$S_{1/3\text{ dB}}(f_c) = 10\log\sum_{f=f_1}^{f_2} S(f), \tag{3}$$

where, $f_1,\ f_2,\ f_c$ are beginning, end and the center frequency of each band, respectively. S the sample-PSDs, and $S_{1/3\text{ dB}}$ the third octave SPD represented by f_c.
Then, for each third octave SPDs, histograms are calculated to represent the associated sound level empirical probability. Those histograms are calculated for three depth layers: 0-350m, 350-650m, 650-1000m. The modelled data are computed to get histograms that match the glider data ones.

Modelled and experimental histograms are compared using three methods.

The mean-square error:

$$\text{MSE}(H_{exp}, H_{model}) = \sqrt{\frac{1}{N}\sum_{i=1}^{N}(H_{exp}(i) - H_{model}(i))^2} \tag{4}$$

where N is the number of bins, and $H_{exp}(i)$ and $H_{\text{model}}(i)$ represent respectively the values of the experimental histogram and modelled histogams at bin i.

The Kullback-Leibler (KL) divergence, that measures how a model probability distribution is different from a true probability distribution, given by:

$$D_{\text{KL}}(H_{\text{exp}}, H_{\text{model}}) = \sum_{i=1}^{N} H_{\text{exp}}(i)\log\frac{H_{\text{exp}}(i)}{H_{\text{model}}(i)} \tag{5}$$

The Jensen-Shannon (JS) divergence is the summation of two KL divergences using a distribution m that is a mix of the model and the experimental distribution. This divergence there is no more the notion of truth included in the KL divergence definition:

$$D_{\text{JS}}(H_{\text{exp}}, H_{\text{model}}) = \frac{1}{2}D_{\text{KL}}(H_{\text{exp}}, n) + \frac{1}{2}D_{\text{KL}}(H_{\text{model}}, n) \tag{6}$$

where n is the average distribution:

$$n(i) = \frac{H_{\mathrm{exp}}(i) + H_{\mathrm{model}}(i)}{2} \tag{7}$$

IV. Results and analysis

Fig.3 shows the two resulting PSD that are clearly distinguishable differences, Fig. 3. The PSD computed using tracks with self-noise is clearly contaminated throughout the mission, while the PSD derived from tracks without self-noise remains clean and reliable and provides a good basis for studying the ambient sound field. By examining the clean PSD, spectral levels show a declining level over the frequency. It is the effect of the higher attenuation for upper frequencies in deep water propagation [21]. Levels are notably strong below 200 Hz where they reach 90 dB compared to 60 dB in the rest of the frequency band, that is a result of flow noise. Within the frequency band $10 - 2000$ Hz, levels vary significantly with the time. This may be due to differences in water column properties or variation in the marine traffic and wind speed conditions. Between 2000 Hz and 3000 Hz two frequencies have lower levels within the whole mission. This is due to unsolved hydrophone calibration issues.

(a)

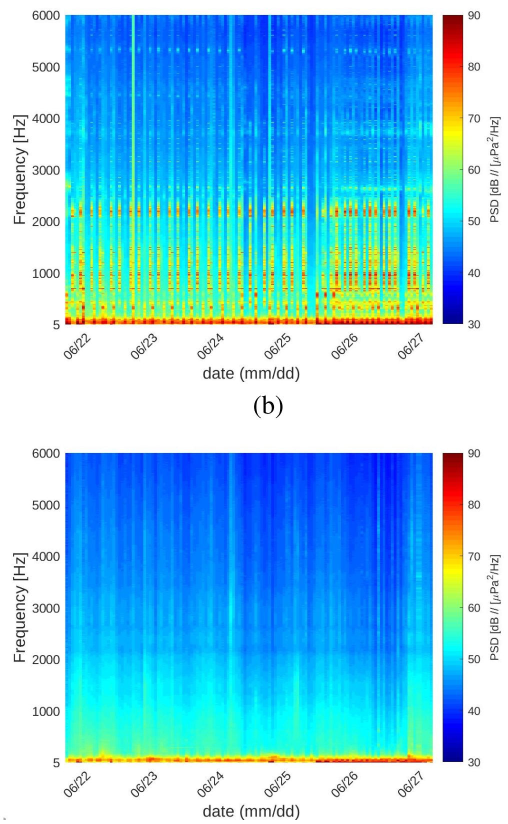

Fig. 3: PSD 1h averaging with self-noise (a), PSD 1h averaging without (b).

Fig. 4 shows the averaged PSD over the frequency band $200 - 1000$ Hz and the wind speed forecast along the glider route provided by the Copernicus database [22]. This frequency band was chosen because wind-generated noise reaches its highest levels at these wind speeds [23]. The wind speed declined from 10 km/h to 7 km/h between June 22 and mid-June 26, as well as the average spectral level, from 52 dB to 46 dB. The corresponding correlation coefficient between those two datasets is $R = 0.65$, which quantifies a clear statistical link between the wind and recorded acoustic data within the selected frequency band. These results suggest that wind-generated noise is a predominant source in the recorded ambient sound field. However, there are some short periods, such as early on June 24 or June 25 afternoon, where the spectral level is not correlated with the wind speed, shown in black dashed rectangles in Fig. 4. This can be due to discrepancies in the Copernicus forecast or other acoustic events such as marine traffic or biological activities that are present in the selected frequency band.

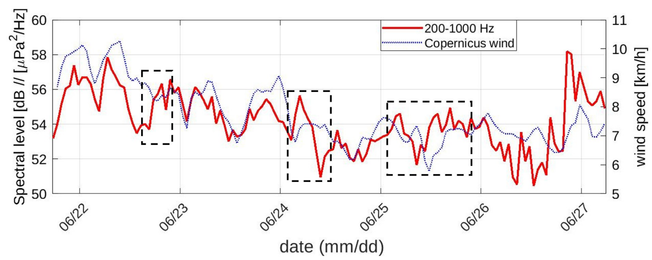

Fig. 4: Mean of the PSD within [200-1000] Hz frequency band (red line), Copernicus wind speed forecast of the glider trajectory during the mission (dashed blue line). Black dashed rectangles show time periods where wind speed and sound level do not correlate.

Fig. 5 shows the SPD during phase 1 where similar features with what is explained in the subsection III-A were found. In fact, SPD frequency axes can be split into three bands. First, above 200 Hz is the ambient sound field region that is decreasing continuously with frequency. It is in agreement with the previous PSD results. Secondly, the flow-noise and ambient sound region between 50 Hz and 200 Hz is characterized by a slope $m = -2.57$, dashed red line on Fig. 5.b, m is defined here as the mean of all percentile slopes between 80 and 200 Hz. At last, the flow noise region, below 50 Hz, does not follow the expected slope $f^{-5/2}$, but a positive one.

The presented results show a frequency band where flow noise is noticeable below 200 Hz, which is narrower than the bands reported in the literature, typically extending below $500\,Hz$. The results are in line with the cited literature for the region characterized by the slope f^{-m}, they presented a narrower e slope $f^{-5/2}$ is not present, but a positive one.

There are discrepancies in the flow noise contribution frequency band between results and cited literature .The observed range is narrower in the present results, below 200 Hz compared to 500 Hz, and the expected slope $f^{-5/2}$ is

absent. This could be due to different water flow conditions. Most of cited studies are in context of strong ocean currents ranging from $1-3$ m/s, while the glider faced an approximate flow of about 0.6 m/s during step 1. This difference may result in a higher flow noise level across a broader frequency band. At last, the absence of the slope $f^{-5/2}$ can be due to the acoustic system high pass filter or the presence of a hydrophone protection at the glider nose.
In Fig. 5.b lower percentiles show which level happens most of the time and follow approximately smooth curves that represent well the flow-noise theory. In contrast, percentiles above the median indicate levels that occurred rarely and show more irregularities across frequency. For example, in the band 5 to 10 Hz, there is a bump for percentiles greater than the median that could be due to transient sound from biological or anthropogenic sources, shown in a black dashed rectangle on Fig. 5.b. The 99^{th} percentile has a singular curve with peaks at each decade from 10 to 50 Hz. It can be caused by a ship passing close to the hydrophone or vibrations of the glider nose that occurred during a period with higher water flow faced by the glider. Studying high percentiles appears to be an effective method for characterizing the ambient sound field in a context of flow noise.

Fig. 6 shows modelled and experimental histograms of June 22 were calculated for 3 depth layers: $0-350$ m, $350-650$ m, $650-1000$ m, figure rows, and for three frequencies, figure columns, that correspond to the three regions characterized by flow noise. In all the chosen frequencies and depth layers, the experimental distributions are centered at a higher level than the modelled ones. Modelled histogram shapes are not Gaussian. The shapes of the experimental histograms are different, Gaussian except for the frequency $f_c = 125$ Hz for mid and up layers.

Fig. 7 shows results of the 3 different validation tests between modelled and experimental histograms. They all exhibit a minimum error between 100 and 500 Hz, as well as a lower error at low than high frequencies, more marked by the MSE than the divergence metrics. The minimum error frequency band overlaps approximately with the wind-generated noise frequency band, and the lower frequency is where acoustic sources of the marine traffic noise model are distributed. It also has to be highlighed, that for the three metrics, error increases with the depth. The validation methods show that the soundscape model tends to be closer to the experimental one in the wind-generated frequency band, then on the marine traffic source frequency band, and stronger differencies at high frequency, where no acoustic source model is prevalent. So, the validation metrics are in line with the model input. At low frequency, the error can be explained by the presence of flow noise in the experimental data as well as acoustic sources distributed in this band and not accounted for the model, such as earthquake noise or cetaceans vocalisation.

(a)

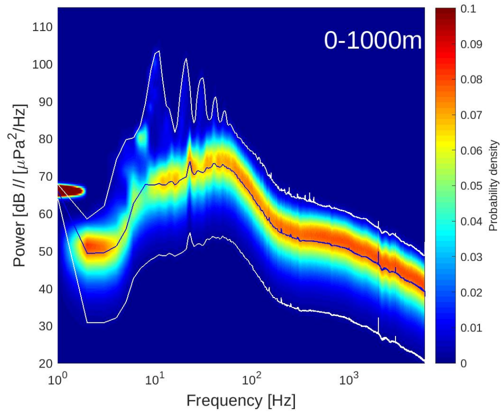

(b)

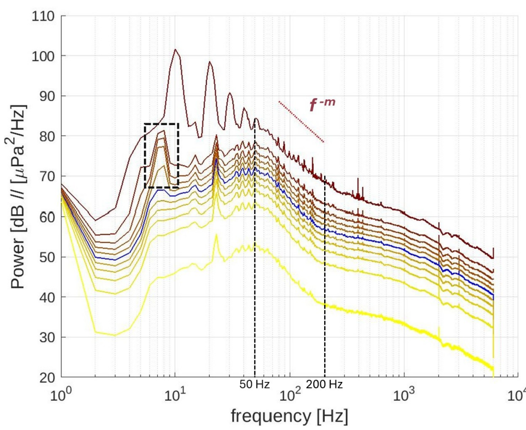

Fig. 5: SPD of the phase with the 1^{st}, 99^{th} percentiles in white, and the median in black (a).SPD percentiles of the phase 1, the 1^{st}, 99^{th} and all the tenth percentiles that comprise the median in blue, the f^{-m} slope in red dashed line (b).

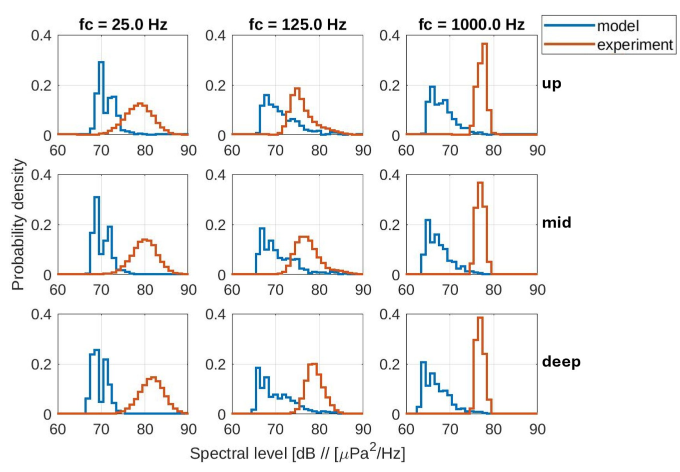

Fig. 6: spectral level probability histograms of 3 1/3 octave frequency bands at 3 depth layers : upper row: $0-350$ m, mid row:$350-650$ m, lower row$650-1000$ m. Modelled histograms are in red, and experimental histograms are in blue.

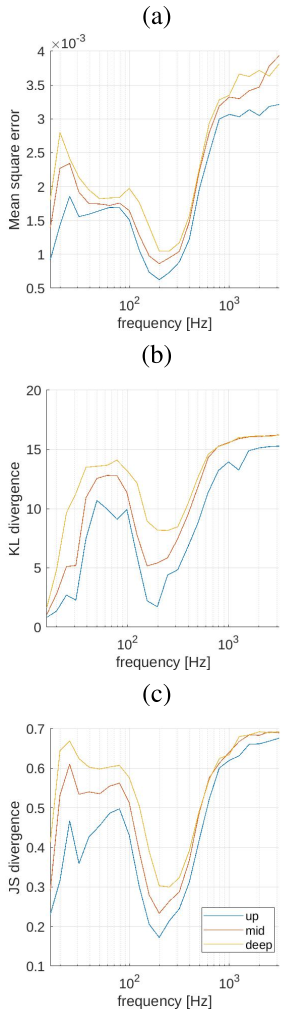

Fig. 7: Histogram validation results over frequencies for the 3 depth layers

V. Conclusion

This study shows how gliders can be used to study the ambient sound field and validate a soundscape model. The primary step was to eliminate the self-noise of the glider that permits to give reliable results to study the ambient sound field. The flow noise was evaluated to be distributed below 200 Hz. Also, a PSD time series was computed showing a ambient sound field dominated by the wind-generated noise. The experimental and modelled histograms were computed and compared. The validation metrics gave results in line with the model features: lower error in frequency bands where acoustic sources were modelled. It also has been highlighted that the ambient sound field can be characterized in a flow noise prevalent context by studying the high percentiles of the SPD. This study proves that gliders are an efficient acoustic recording platform to monitor a soundscape. First, gliders enable data collection along chosen trajectories, down to 1000 m, allowing model comparisons on a regional scale. Second, gliders after a low frequency, in this case 200 Hz do not generate flow noise and collect data soundlessly, this frequency could be lowered by reducing the glider speed. In a context of deep-sea activities monitoring, this method proved to be valuable for obtaining far-field data over extensive regions as a complement to fixed hydrophones, which are more suited for near-field and mid-field monitoring.

References

[1] B. Ramiro-Sánchez, J. M. González-Irusta, L.-A. Henry, J. Cleland, I. Yeo, J. R. Xavier, M. Carreiro-Silva, I. Sampaio, J. Spearman, L. Victorero, C. G. Messing, G. Kazanidis, J. M. Roberts, and B. Murton, "Characterization and mapping of a deep-sea sponge ground on the tropic seamount (northeast tropical atlantic): implications for spatial management in the high seas," *Frontiers in Marine Science*, vol. 6, May 2019.

[2] R. Williams, C. Erbe, A. Duncan, K. Nielsen, T. Washburn, and C. Smith, "Noise from deep-sea mining may span vast ocean areas," *Science*, vol. 377, p. 157–158, July 2022.

[3] D. D. J. A. D. M. Cyrill Martin, Dr. Lindy Weilgart, "Deep-sea mining: a noisy affair," *OceanCare*, vol. 1, 2021.

[4] E. Silva, D. Viegas, A. Martins, J. Almeida, C. Almeida, B. Neves, P. Madureira, A. Wheeler, G. Salavasidis, A. Phillips, A. Schaap, B. Murton, A. Berry, A. Weir, G. Dooly, E. Omerdic, D. Toal, P. Collins, M. Miranda, C. Petrioli, C. Barrera Rodríguez, D. Demoor, C. Drouet, G. Serafy, S. Jesus, J. Dañobeitia, V. Tegas, S. Cusi, L. Lopes, B. Bodo, L. Beguery, S. VanDam, J. Dumortier, L. Neves, V. Srivastava, T. Dahlgren, J. Thomassen Hestetun, R. Eiras, R. Caldeira, C. Rossi, J. Spearman, L. Somoza, F. González, R. Bartolomé, and P. Bahurel, "Trident – technology based impact assessment tool for sustainable, transparent deep sea mining exploration and exploitation: a project overview," in *OCEANS 2023 - Limerick*, p. 1–7, IEEE, June 2023.

[5] W. Cornwall, "Sunken summits," *Science*, vol. 365, no. 6458, pp. pp. 1104–1107, 2019.

[6] L. de Oliveira Júnior, O. C. Rodríguez, and S. M. Jesus, "Ocean noise field-calibration constraints for deep sea mining," in *OCEANS 2024 - Singapore*, p. 01–05, IEEE, Apr. 2024.

[7] J. H. Haxel, H. Matsumoto, C. Meinig, G. Kalbach, T.-K. Lau, R. P. Dziak, and S. Stalin, "Ocean sound levels in the northeast pacific recorded from an autonomous underwater glider," *PLOS ONE*, vol. 14, p. e0225325, Nov. 2019.

[8] R. A. S. Gehrmann, D. R. Barclay, H. Johnson, N. Shajahan, V. Nolet, and K. T. A. Davies, "Ambient noise levels with depth from an underwater glider survey across shipping lanes in the gulf of st. lawrence, canada," *The Journal of the Acoustical Society of America*, vol. 154, p. 1735–1745, Sept. 2023.

[9] P. Cauchy, K. J. Heywood, N. D. Merchant, D. Risch, B. Y. Queste, and P. Testor, "Gliders for passive acoustic monitoring of the oceanic environment," *Frontiers in Remote Sensing*, vol. 4, Feb. 2023.

[10] M. Strasberg, "Nonacoustic noise interference in measurements of infrasonic ambient noise," *The Journal of the Acoustical Society of America*, vol. 66, p. 1487–1493, Nov. 1979.

[11] C. Erbe, A. Verma, R. McCauley, A. Gavrilov, and I. Parnum, "The marine soundscape of the perth canyon," *Progress in Oceanography*, vol. 137, p. 38–51, Sept. 2015.

[12] C. Bassett, J. Thomson, P. H. Dahl, and B. Polagye, "Flow-noise and turbulence in two tidal channels," *The Journal of the Acoustical Society of America*, vol. 135, p. 1764–1774, Apr. 2014.

[13] M. F. Auvinen, D. R. Barclay, and M. E. W. Coffin, "Performance of a passive acoustic linear array in a tidal channel," *IEEE Journal of Oceanic Engineering*, vol. 45, p. 1564–1573, Oct. 2020.

[14] A. Agrawal, R. Kumar, and M. Agrawal, "Modeling of underwater noise," in *OCEANS 2019 - Marseille*, p. 1–6, IEEE, June 2019.

[15] M. Zhou, J. Wang, X. Feng, H. Sun, J. Li, and X. Kuai, "On generative-adversarial-network-based underwater acoustic noise modeling," *IEEE Transactions on Vehicular Technology*, vol. 70, p. 9555–9559, Sept. 2021.

[16] Copernicus Marine Service, "Global ocean physics analysis and forecast." https://data.marine.copernicus.eu/product/GLOBAL_ANALYSISFORECAST_PHY_001_024/description, 2025. Accessed: 2025-04-09.

[17] GEBCO Compilation Group, "Gebco gridded bathymetry data." https://www.gebco.net/data_and_products/gridded_bathymetry_data/, 2025. Accessed: 2025-04-09.

[18] M. Porter, "Bellhop3d user guide," technical report, HLS Research, 2016. Tech. Rep.

[19] A. MacGillivray and C. de Jong, "A reference spectrum model for estimating source levels of marine shipping based on automated identification system data," *Journal of Marine Science and Engineering*, vol. 9, p. 369, Mar. 2021.

[20] J. A. Hildebrand, K. E. Frasier, S. Baumann-Pickering, and S. M. Wiggins, "An empirical model for wind-generated ocean noise," *The Journal of the Acoustical Society of America*, vol. 149, p. 4516–4533, June 2021.

[21] R. J. Urick, *Principles of underwater sound*. New York: McGraw-Hill, 3rd ed., 1983.

[22] Copernicus Marine Service, "Global ocean wind l4 near real time observations." https://data.marine.copernicus.eu/product/WIND_GLO_PHY_L4_NRT_012_004/description, 2025. Accessed: 2025-04-09.

[23] G. M. Wenz, "Acoustic ambient noise in the ocean: spectra and sources," *The Journal of the Acoustical Society of America*, vol. 34, p. 1936–1956, Dec. 1962.